Received: 3 July 2025 | Revised: 8 July 2025 | Accepted: 19 August 2025

DOI: 10.1002/aic.70062

RESEARCH ARTICLE

Transport Phenomena and Fluid Mechanics

AIChE JOURNAL

Improving wet scrubber efficiency using fiber-guided drops

Chase T. Gabbard[1] | James T. Rhoads[2] | Joshua B. Bostwick[2] | J. R. Saylor[2]

[1]School of Engineering, Brown University, Providence, Rhode Island, USA

[2]Department of Mechanical Engineering, Clemson University, Clemson, South Carolina, USA

Correspondence
J. R. Saylor, Department of Mechanical Engineering, Clemson University, Clemson, SC, USA.
Email: jsaylor@clemson.edu

Funding information
Clemson University

Abstract

Wet scrubbers are widely used to mitigate fossil fuel emissions, making improvements in their efficiency an impactful pursuit. In this study, we analyze an atypical approach to liquid distribution in wet scrubbers that uses liquid drops flowing down vertical fibers which offers several benefits. These include extended residence time, reduced pressure drop, monodisperse drop size distributions and tunability of all of these, including the drop number density. The residence time and drop number density are the most significant of the aforementioned effects and are strongly affected by viscosity. Accordingly, we chose to study silicone oils, available in a range of viscosities, to investigate the scavenging coefficient of fiber-guided drops, and demonstrate their potential to enhance wet scrubber performance. Additionally, we identify optimal system parameters for effectively capturing particles across a range of particle diameters, paving the way for more efficient wet scrubbers.

KEYWORDS
bead-on-fiber flow, drop dynamics, Greenfield gap, particle scavenging, wet scrubber

1 | INTRODUCTION

Air pollution is a major global health risk, with airborne particulate matter ranking as the 13th leading cause of death worldwide.[1] In nature, falling raindrops improve air quality by removing aerosols from the atmosphere and scavenging pollutants.[2–4] Engineered attempts to scrub airborne particulate often mimic this mechanism by using falling drops to capture and remove airborne particles. These systems are ubiquitous in industry where they protect public health by removing a myriad of anthropogenic pollutants, including volatile organic compounds from rubber emissions,[5] toxic fine particles generated by the foundry industry,[6] long-lived radioactive dust in uranium mines,[7] and gases and particulate from fossil fuel power plants. By replicating the particle-collection ability of natural raindrops, wet scrubbers clean polluted gas streams using downward-directed water sprays, capturing and removing particles with high efficiency.[8] Recently, Sadeghpour et al.[9] introduced a wet electrostatic precipitator that used water drops flowing down a vertical fiber to remove particulate matter instead of free-falling drops. Their system achieved over 80% collection efficiency for a wide range of particle sizes, and reduced pressure drop by up to two orders of magnitude compared to conventional collection methods. Building on their work, we investigate how liquid viscosity and drop number density influence particle collection efficiency of liquid drops flowing down a fiber guide.

1.1 | Particle scavenging

Scrubbers comprise a large range of devices incorporating a diversity of approaches for removing something undesirable from a fluid flow.[10] For example, scrubbers remove gases[11] and aerosols[6] from a gas stream, and include systems that use electrostatic precipitators to enhance particle removal from a gas,[12] devices wherein the gas is bubbled upward through the liquid,[13] and devices that include a Venturi throat that atomizes a liquid inlet flow, creating a large number of drops that remove pollutants,[14] to name just a few. Here we focus on scrubbers that utilize downward falling drops to remove aerosols, and seek to determine how a fiber guide may improve performance.

Particle scavenging by a scrubber may be quantified by the scavenging coefficient

$$E_p = \frac{C_i - C_e}{C_i}, \tag{1}$$

where C is the particle number density and i and e refer to the inlet and exit of the scrubber, respectively. Note that C may be the number density for a single particle diameter or the total number density for all measurable particle diameters.

Small particles are primarily collected by Brownian motion, while larger particles are captured via inertial impaction.[15] Although additional mechanisms such as phoretic effects exist,[16] we follow the treatment of Wang et al.[17] and only consider particle removal due to Brownian diffusion, inertia, and interception, the process whereby a particle that follows a streamline that is less than one particle radius from the drop is captured. Under these conditions,

$$E_p = 1 - e^{-\Lambda_p t_r} \tag{2}$$

where t_r is the residence time of the drop and Λ_p is the fractional particle removal rate[17,18]:

$$\Lambda_p(d_p) = \int_0^\infty \frac{\pi}{4}(d_p + d_d)^2 (V(d_d) - v(d_p)) Z(d_p, d_d) N(d_d) d(d_d). \tag{3}$$

Here, d_d and d_p are the drop and particle diameters, $N(d_d)$ is the drop size distribution, $V(d_d)$ and $v(d_p)$ are the terminal velocities of the drop and particle, and $Z(d_p, d_d)$ is the collection efficiency, expressed as[17]:

$$\begin{aligned} Z(d_p, d_d) = {} & \frac{4}{\mathrm{Re\,Sc}}\left(1 + 0.4\,\mathrm{Re}^{1/2}\mathrm{Sc}^{1/3} + 0.16\,\mathrm{Re}^{1/2}\mathrm{Sc}^{1/2}\right) \\ & + \frac{4d_p}{d_d}\left(\frac{\mu_a}{\mu_d} + \left(1 + 2\mathrm{Re}^{1/2}\right)\frac{d_p}{d_d}\right) \\ & + \left(\frac{\mathrm{St} - \mathrm{St}^*}{\mathrm{St} - \mathrm{St}^* + 2/3}\right), \end{aligned} \tag{4}$$

where the first, second, and third terms correspond to collection by Brownian diffusion, interception, and inertial impaction, respectively. The Reynolds and Schmidt numbers are given by:

$$Re = \frac{\rho_a d_d V(d_d)}{2\mu_a}, \tag{5}$$

$$Sc = \frac{\mu_a}{\rho_a \mathcal{D}}, \tag{6}$$

with the effective diffusion coefficient $\mathcal{D}$ defined as

$$\mathcal{D} = \frac{k_b T C_c}{3\pi\mu_a d_p}, \tag{7}$$

and the Cunningham correction factor

$$C_c = 1 + \frac{2.52\alpha}{d_p} \tag{8}$$

where k_b is Boltzmann's constant, T is temperature, μ_a is the dynamic viscosity of the air, and α is the mean free path of air. The particle Stokes number St is

$$St = \frac{2\tau(V(d_d) - v(d_p))}{d_d}, \tag{9}$$

with the particle relaxation time τ given by

$$\tau = \frac{(\rho_p - \rho_a) d_p^2 C_c}{18\mu_a}. \tag{10}$$

The modified Stokes number St^* is

$$St^* = \frac{1.2 + \frac{1}{12}\ln(1 + Re)}{1 + \ln(1 + Re)}. \tag{11}$$

In all expressions, ρ_p is the particle density, ρ_a is the air density, and μ_d is the dynamic viscosity of the drop, and g is the gravitational acceleration. Note that the inertial term in Equation (4) is set to zero if $St^* > St$. When nonzero, this term is multiplied by $\rho_p/1000$ for particles denser than water.

The equation used for terminal velocity depends on the diameter of the falling object. Here, we assume that the particles are small, and hence we use a terminal velocity equation based on Stokes flow for these particles:

$$v(d_p) = \frac{d_p^2(\rho_p - \rho_a) g C_c}{18\mu_a}. \tag{12}$$

Additionally, we assume the drops are relatively large, on the order of millimeters, and adopt the empirical terminal velocity correlation of Atlas and Ulbrich[19]

$$V(d_d) = 386.6 d_d^{0.67}. \tag{13}$$

The significance of Equations (3) to (11) is their role in determining Λ_p, which contributes to the exponential term in Equation (2). To estimate how Λ_p scales with drop size, we perform an order-of-magnitude analysis. Assuming $d_d \gg d_p$, $v(d_p) \approx 0$, and $\rho_d \gg \rho_a$, we find that $\Lambda_p \sim \mathcal{O}(d_d^{2.67})$ for fixed particle diameter, temperature, and drop number density. This almost-cubic increase is moderated by two effects. First, at fixed drop number density Γ, increasing d_d leads to a cubic increase in drop mass and thus in the total mass flow rate, increasing pumping power requirements. Second, and the subject of this work, the scavenging efficiency Equation (2) depends on the product $\Lambda_p t_r$, where t_r is the residence time of a drop in a scrubber of height $\mathcal{L}$:

$$t_r = \mathcal{L}/V(d_d), \tag{14}$$

Using the scaling $V(d_d) \sim d_d^{0.67}$ from Equation (13), this reduces the scaling of $\Lambda_p t_r$ to $\sim d_d^2$. Therefore, while Λ_p increases with drop size, the residence time decreases, partially offsetting the benefit. Taking this into consideration, E_p scales as drop diameter squared, suggesting that improved scavenging could be obtained simply by using large drops. But, again, this is offset by the required pumping power which scales as diameter cubed.

Increasing t_r is a promising route to improved efficiency but is practically limited by the height of the scrubber. For example, with $\mathcal{L} \sim 1$ m and $d_d \sim 1$ mm, Equation (13) gives $V(d_d) \sim 1$ m/s, yielding a residence time on the order of one second. A higher residence time t_r may be achieved by incorporating an upward air flow. However, this would demand greater blower energy and introduce inefficiencies, as drops would quickly aggregate and fall due to their increased mass. Furthermore, the inlet nozzles in scrubbers produce polydisperse sprays, where larger drops fall swiftly and smaller drops are carried out by the gas flow, reducing the number of drops available for particle capture.

1.2 | Fiber-guided drops

An effective strategy to slow drops and address issues like high energy costs in wet scrubbers is to guide liquid along a vertical fiber, creating a bead-on-fiber flow. Hereinafter we shall call these beads, fiber-guided drops, or simply fiber drops. These fiber drops emerge naturally from capillary instability, which breaks the cylindrical liquid sheath into drops descending the fiber, similar to the Plateau–Rayleigh instability.[20,21] The spacing between fiber drops λ can be tuned via flowrate Q,[22] enabling control of drop density along fibers. In this system, the drop number density Γ is the product of $1/\lambda$ and the number of fibers per unit area, N_A, which can also be controlled by structuring the fiber array. Fiber drops are generally monodisperse and their velocity V_b and retention time can be controlled through the liquid viscosity μ, offering a tunable method of liquid distribution. This approach has found application in heat and mass transfer,[23,24] CO_2 separation,[25–27] desalination,[28,29] and ultra-fine particle scavenging.[9]

Drops flowing along a vertical fiber can produce steady and unsteady patterns.[23,30] At low Q and small fiber radius R, drops form uniformly and travel independently. As either Q or R increases, drops interact and become polydisperse, marking a transition from absolute to convective instability.[31,32] Drop patterns may also lose their axisymmetry, either due to fluid–fiber properties, fiber eccentricity, or external forcing.[33–36] When the drop pattern is steady, several useful empirical trends are known, such as d_d increases with nozzle radius R_n, decreases with R, and has a weak non-monotonic dependence on Q.[22,37] The velocity of a fiber drop increases with its size but is damped by viscous drag,[22,38] while the spacing between drops λ is mostly tuned through Q. Together, the spacing and velocity define the drop frequency $f = V_b/\lambda$ which is a useful metric that has been studied in detail for symmetric and asymmetric fiber drop patterns.[39] In addition to the numerous empirical trends and scaling arguments previously reported, a number of models have also been developed,[40–45] making fiber drops a well-characterized mode of liquid delivery.

Fiber-guided drops were first explored as a means for improved liquid delivery in heat recovery from exhaust gas.[23] In addition to their high efficiency, fiber drop patterns have a streamlined shape, allowing them to reduce gas-side pressure drop by orders of magnitude compared to commercial systems.[24,26,28,46] The drop number density Γ in these applications is easily adjusted through the spacing between neighboring fibers and the spacing between drops on the same fiber λ. When the drop pattern is steady, the spacing between drops is constant along the fiber and tuned using the liquid flowrate Q, with smaller λ, and thus higher Γ, being advantageous for several applications, including water desalination.[28] In contrast, some applications benefit from unsteady patterns, such as direct-contact heat exchangers.[47] The practical utility of fiber drops have also been tested for many functional liquids such as MEA[24–26] and polyvinylpyrrolidone,[48] and under low to moderate gas counterflows.[26,49]

In particle scavenging, Ali et al.[50] developed a wet electrostatic precipitator using liquid flowing down a permeable rope in a counterflow configuration, achieving over 80% collection efficiency for micron-sized particles. Building on this concept, Sadeghpour et al.[9] introduced an electrostatic precipitator design in which drops flow down a fiber. They tested particles spanning three orders of magnitude in diameter and flowrates across two orders of magnitude. Their design outperformed several existing alternatives while significantly reducing the liquid-to-air flowrate ratio. Efficiency improved with applied voltage, though strong counterflow diminished performance. Together, these studies highlight the potential of fiber-guided drops for wet scrubber applications. However, two key parameters that govern collection efficiency, the residence time, which can be tuned by the liquid viscosity μ, and the drop number density Γ, which depends on drop spacing, have not yet been systematically explored and are the focus of this study.

1.3 | Outline

In this paper, we present a combined experimental and numerical investigation of particle collection by fiber-guided drops. Section 2 outlines the experimental setup, and Section 3 details the simulation methodology. In Section 4.1, we present the global scavenging curves, followed by an analysis of how key features vary with viscosity and drop spacing in Section 4.2. Section 5 introduces a data collapse for the collection efficiency based on the residence time t_r and drop number density Γ, and explores the broader implications. We conclude in Section 6 by summarizing our findings and outlining the steps needed to implement fiber-guided drops for improving wet scrubber performance in real-world applications.

2 | EXPERIMENTAL METHOD

We performed experiments using the setup shown in Figure 1A. A syringe pump (NE-1000, New Era Pump Systems) was operated at flowrate $Q = 27.8 - 166.7$ mm^3/hr, pumping liquid through a stainless

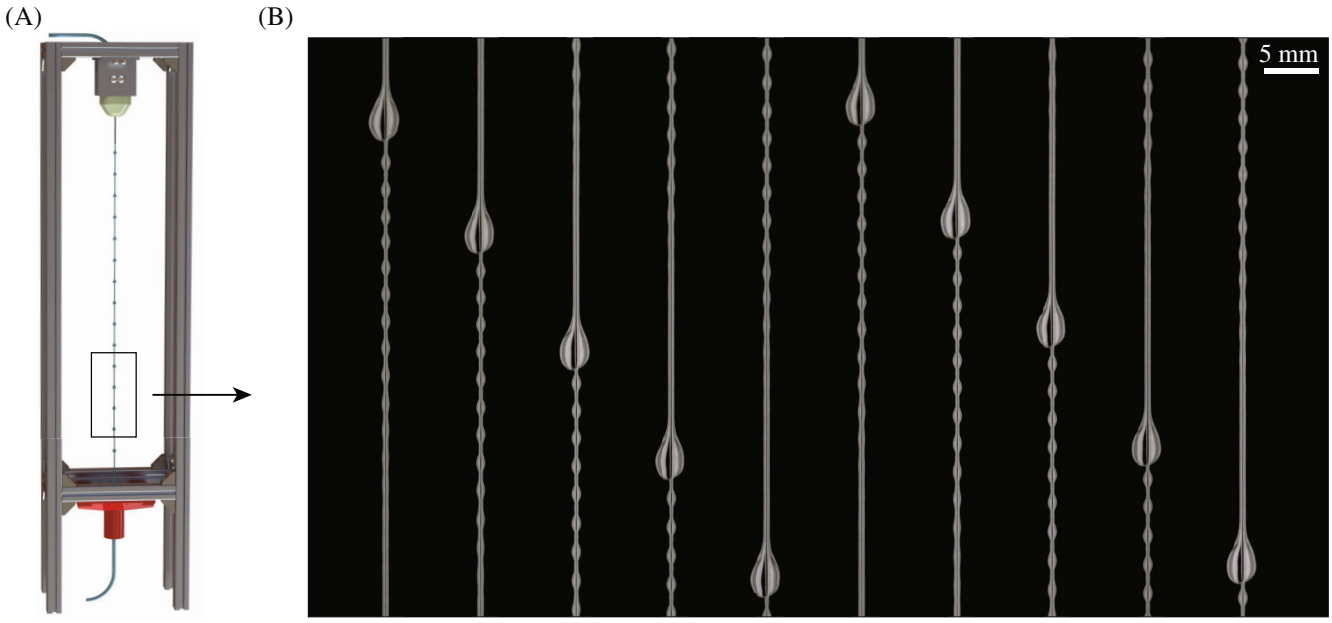

FIGURE 1 (A) The experimental setup and (B) an image sequence from a typical experiment for silicone oil $\mu = 9.4$ mPa s on a nylon fiber $R = 0.1$ mm. Images advance by 0.04 s from left to right.

steel nozzle with radius $R_n = 0.6$ mm and onto a nylon fiber with radius $R = 0.1$ mm. The nozzle and fiber were mechanically aligned using a resin-printed housing. The working liquid was silicone oil with viscosity $\mu = 4.58$ mPa s (Esco Products) and $\mu = 0.816$ mPa s (Clearco Products), and with density $\rho = 816 - 915$ kg/m^3 and surface tension $\sigma = 17.4 - 20.0$ mN/m. The liquid properties were either supplied by the manufacturer or measured using an Attension Sigma 702 force tensiometer with Wilhelmy plate and density probe, for σ and ρ, respectively, and an Anton Paar MCR 302 cone-plate rheometer for μ.

Liquid deposited onto the vertical fiber readily destabilized into periodic drops that flowed at steady-state following a brief transient period. The flow dynamics were fully resolved by recording the drops with a Chronos 2.1-HD high speed camera (Kron Technologies) at a frame rate of 2996 fps and 12,075 fps. A typical experiment is shown in Figure 1B for silicone oil ($\mu = 9.4$ mPa s) with time increasing from left to right. In addition to the large flowing drops that are the focus of this study, smaller secondary drops can form when the drop passage frequency and liquid viscosity are small. The drops were identified and tracked using a custom MATLAB script. The measured properties were the drop diameter d_d, velocity V_d, and the spacing between subsequent drops λ. We restricted our experiments to flowrates that produce steady drop patterns, so the measured variables were nearly constant and we report the average value from tracking 20 or more drops.

To thoroughly explore the role of viscosity on particle scavenging, we combine the present low-viscosity experiments with the higher-viscosity experiments presented in Gabbard and Bostwick.[22] The interested reader is directed to this prior work for a detailed account of the experiments, but we present the salient points below. The working fluid was silicone oil with viscosity $\mu = 0.0094 - 0.974$ Pa s, density $\rho = 967 - 974$ kg/m^3, and surface tension $\sigma = 0.022$ N/m. Stainless steel nozzles with radius $R_n = 0.2 - 1.65$ mm were used to deposit liquid onto nylon fibers with radius $R \approx 0.05 - 0.25$ mm. The same liquid-fiber properties between these experiments and those in the present work ensure similar wettability across the comprehensive dataset. The range of fluid properties, fiber sizes, and flowrates analyzed in this study are given in Table 1.

3 | SIMULATIONS

Values of E_p were obtained by solving Equations (2) to (14) for each drop-on-fiber experiment. The experimental data provided the drop diameter d_d, the drop velocity V_d, which is used as the terminal velocity instead of Equation (13), and the spacing between drops, λ which gave the drop number density $\Gamma = N(d_d) = N_A(d_d)/\lambda$ where $N_A(d_d)$ is the presumed drops per unit area (identical to the number of fibers per unit area in a presumed scavenging system), and which was set to 10^4/m^2 to ensure the pitch between fibers is large enough to avoid forming liquid bridges.[51,52] Values for λ were typically on the order a centimeter, giving a typical drop number density Γ on the order of 10^6/m^3 or one drop per cubic centimeter.

Simulations were performed for particle diameters $d_p = 10^{-3}$–$10^3 \mu$m. All simulations ignore drop-drop or particle-particle interactions. In some cases, we simulated the collection efficiency of a free-falling water drop for comparison with fiber-guided drops, with the terminal velocity given by Equation 13. For these, we assumed the water drops are falling at their terminal velocity. The fiber drops were presumed to fall precisely as a free falling drop, except with the descent velocity measured in experiment. In other

TABLE 1 Parameter ranges.

Parameter	Symbol	Units	Range
Density	ρ	kg m^{-3}	816 – 974
Viscosity	μ	mPa s	0.816 – 974
Surface tension	σ	mN m^{-1}	17.4 – 22.0
Fiber radius	R	mm	0.5 – 2.5
Flowrate	Q	mm^3 s^{-1}	2.8–166.7

words, any effect of the fiber on the flow around the drop is ignored. The particle velocity was computed as the terminal velocity from Stokes flow Equation (12) with the Cunningham correction factor C_c applied.

To isolate the effect of the fiber, we additionally simulated the collection efficiency E_{pw} for freely falling water drops with the same diameter and spacing λ as the fiber-guided drops. Comparing E_p to E_{pw} highlights the relative performance of fiber-guided scavenging versus conventional droplet-based approaches. In both cases, the residence time t_r was computed using an arbitrary fiber length (scrubber height) of $\mathcal{L} = 1$ m. Finally, we only accounted for capture by the primary descending drops along the fiber, excluding contributions from the smaller secondary drops (see Figure 1B), which may provide additional scrubbing and are discussed Section 5.

4 | RESULTS

Figure 2 shows the scavenging coefficient E_p plotted against particle diameter d_p for a fiber-guided drop with diameter $d_d = 2.79$ mm and viscosity $\mu = 48$*m*Pa s, and a freely falling water drop $d_d = 2.0$ mm. The curves share a common structure that highlights key features relevant to scrubbing performance. At small and large particle diameters, E_p is high due to Brownian diffusion and inertial capture, respectively. Between these regimes lies a broad efficiency dip known as the Greenfield gap,[2] where neither mechanism is effective. We will refer to this minimum in E_p as the first minimum E_{p1}, which occurs at a particle size d_{p1}. A second local minimum in E_p occurs at larger d_p, where the terminal velocity of the particle and drop equal and scavenging becomes purely diffusive. Because d_p is typically large where the velocities become equal, the diffusive scavenging contribution is small. We will refer to this local minimum as the second minimum E_{p2}, which occurs at a particle size d_{p2}. Notably, the fine structure of the scavenging curve about E_{p2} requires a high resolution in particle diameter. Although increasing this resolution can more accurately determine E_{p2} our interest lies less in the value of this very low scavenging coefficient and more with its location, d_{p2}, which is our focus.

Finally, it should be noted that the magnitude of E_p in Figure 2 is arbitrary for the freely falling water drops because the drop number density was chosen arbitrarily, unlike for the silicone oil drops where the number density was determined partially by the measured drop spacing on the fiber (although in both cases, the drop areal density N_A is arbitrary).

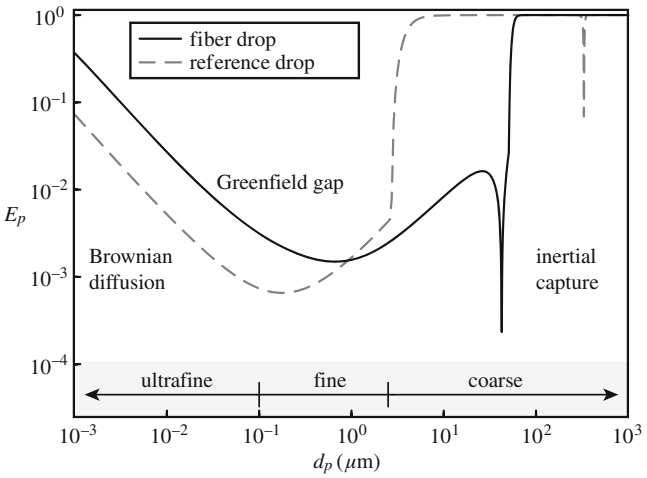

FIGURE 2 Particle scavenging coefficient E_p versus particle diameter d_p for a silicone oil drop with diameter $d_d = 2.79$ mm and viscosity $\mu = 48$ *m*Pa s sliding down a fiber $R = 0.1$ mm, and a free-falling water drop with diameter $d_d = 2.0$ mm. Regions relevant to particle scavenging are labeled, and the particulate size categories are shown along the bottom of the plot.

The first (second) minimum of E_p occurs at larger (smaller) d_p for the fiber-guided drop, since its velocity is slowed by viscous shear at the liquid–fiber interface. This causes the particle range where diffusive capture is effective to shift toward higher d_p, increasing scrubbing performance for small particle sizes. Also, the smaller velocity of the fiber drop means a smaller particle size will have equal velocity, and hence d_{p2} is smaller, as shown in Figure 2. Note that discontinuities may be observed in this and subsequent plots due to the change in regime with drop or particle diameter in the equations presented above (cf. the text after Equation (11)).

Along the bottom of Figure 2, particle sizes are categorized as ultrafine ($< 0.1\,\mu$m), fine (0.1–2.5 μm), and coarse ($> 2.5\,\mu$m). From a human health perspective, ultrafine and fine particles are the most critical to remove as they can most easily invade the respiratory system.[53] Unfortunately, these sizes are both prevalent in industrial emissions—such as diesel particulate matter[54]—and fall within the Greenfield gap where commercial wet scrubbers with freely falling drops are least effective. The need to improve scavenging in this range is underscored by regulatory efforts from agencies like the U.S. Environmental Protection Agency,[55] motivating our reference to these size ranges to contextualize these results.

4.1 | Scavenging curves: Viscous effects

In Figure 3A, we plot the particle scavenging coefficient E_p as a function of particle diameter d_p for each viscosity tested. For clarity, only one representative curve is shown per viscosity, and increasing viscosity is indicated by a color gradient from dark blue to light yellow. To complement our silicone oil data, a fiber drop made of water and flowing on a fiber with radius $R = 0.5$ mm is included as a black dashed

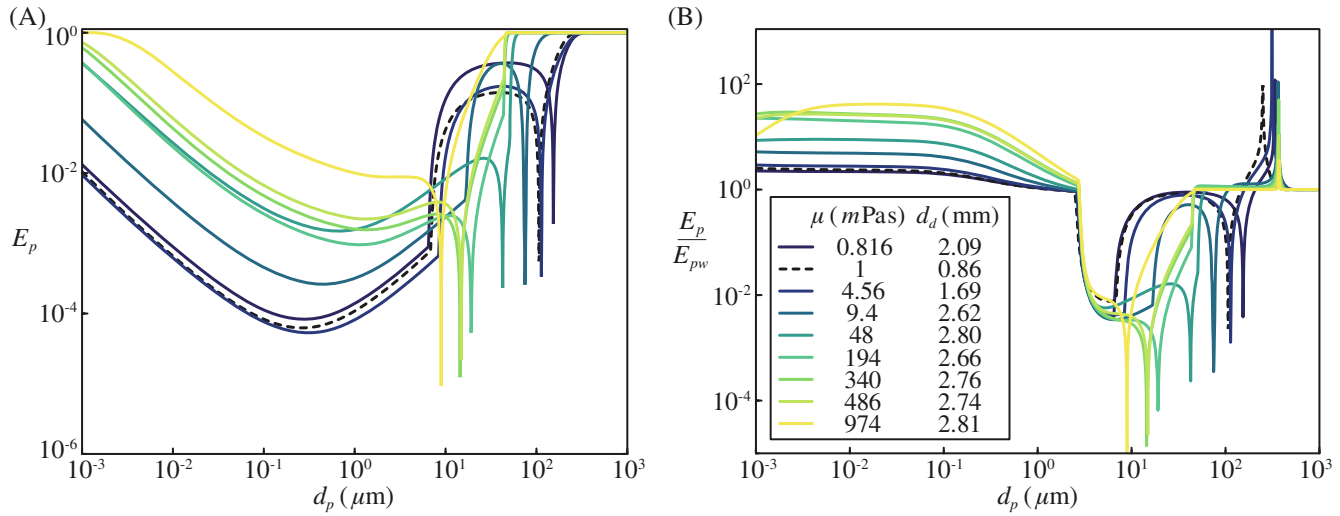

FIGURE 3 (A) Particle scavenging coefficient E_p and (B) E_p normalized by the free-falling drop coefficient E_{pw}, against particle diameter d_p for drops with $R = 0.1$ mm and increasing viscosity μ (dark blue to light yellow). The black dashed line shows water drop data from Grünig et al.[48] for $R = 0.5$ mm.

line and comes from the experiments of Grünig et al.[48] In general, the scavenging curves are similar and shifted upward as μ increases. This increase, enhances scavenging at the first minimum E_{p1} and increases d_{p1}. Increasing viscosity also shifts the second minimum E_{p2} to smaller particle sizes d_{p2}, as a highly viscous fiber drop moves slower. The increase in d_{p1} and decreases in d_{p2} as μ increases brings the minima together, which can become nearly identical, as shown for the highest viscosity case (light yellow). These results suggest that viscosity enhances particle scavenging in the fine and ultrafine particle ranges through two means: by increasing E_p everywhere within the Greenfield gap, and by increasing d_{p1}, allowing smaller particles to be captured with higher efficiency.

To isolate the role of the fiber, Figure 3B shows the relative scavenging coefficient E_p/E_{pw} plotted against d_p, where E_{pw} is the scavenging coefficient for a water drop having the same diameter and number density as the fiber drop, but with a terminal velocity associated with free fall. The values of this scaled metric are greater than one across the ultrafine range ($d_p < 0.1\mu$m) and part of the fine range, indicating improved scavenging due to the increased residence time of the fiber drops. Above these particle sizes, the higher inertia of the freely falling drop provides it superior scavenging in the inertial capture regime, although excessive inertia can inhibit capture.[56] Thus, the fiber-guided approach is more effective at capturing the particle sizes most regulated in industrial emissions and most harmful to human health for the fluids and drop sizes considered here.

4.2 | First and second scavenging minimum

Though E_{p1} and E_{p2} are minima, and therefore correspond to particle diameters that are particularly difficult to capture, they may be shifted to larger or smaller particle diameters by altering the viscosity of fiber-guided drops. Figure 4A is a plot of the first minimum d_{p1} versus viscosity μ for all of our experimental data. The marker colors match those previously used to indicate viscosity, with the black marker representing the water drop case from Grünig et al.[48] A gray dashed line and gray dot-dashed line indicate the coarse-to-fine particle transition and ultrafine-to-fine particle transition, respectively. At low liquid viscosities, $d_{p1} \approx 0.3\,\mu$m, falling within the Greenfield gap. As μ increases, d_{p1} shifts to larger sizes, reaching the coarse particle range for the highest-viscosity drops. This shift helps extend the diffusion-dominated regime to include particles that are most critical for removal. The trend can be understood by identifying where both inertial and diffusive capture mechanisms are weak and of comparable strength. Inertial capture becomes ineffective when the Stokes number St (Equation 9) is small. Assuming the drop velocity dominates over the particle velocity ($V_d \gg v$), the Stokes number scales as $St \sim \left(d_p^2 V_d\right)/(\mu_a d_d)$. For fiber-guided drops, V_d decreases with viscosity as $V_d \sim 1/\mu$. Assuming the drop diameter d_d and air viscosity μ_a are approximately constant, we obtain $St \sim d_p^2/\mu$. On the other hand, diffusion is weak when the Schmidt number Sc (Equation 6) is large. Since $Sc \sim 1/\mathcal{D}$ and the diffusion coefficient $\mathcal{D} \sim 1/d_p$, we find $Sc \sim d_p$. Balancing the conditions where both mechanisms are equally weak, that is, $Sc \sim 1/St$, gives $d_{p1} \sim \mu^{1/3}$. The solid black line in Figure 4A shows the predicted slope of this trend, which captures the overall trend in the data, except at low liquid viscosities, where shear at the air-liquid boundary becomes significant, slowing the drop and modifying the expected scaling behavior.

Figure 4B plots the particle size at the second minimum d_{p2} against viscosity μ. The data follow a decreasing linear trend that reflects the condition $V_d = v$. Since the drop velocity decreases with viscosity as $V_d \sim 1/\mu$, and the particle velocity increases with size as $v \sim d_p^2$ (Equation 12), the scaling relation from equating these is $d_{p2} \sim \mu^{-1/2}$. The slope of this prediction is shown as a solid black line in Figure 4B and closely resembles the trend of the data. The only significant deviation occurs at low viscosities, where, again, interfacial

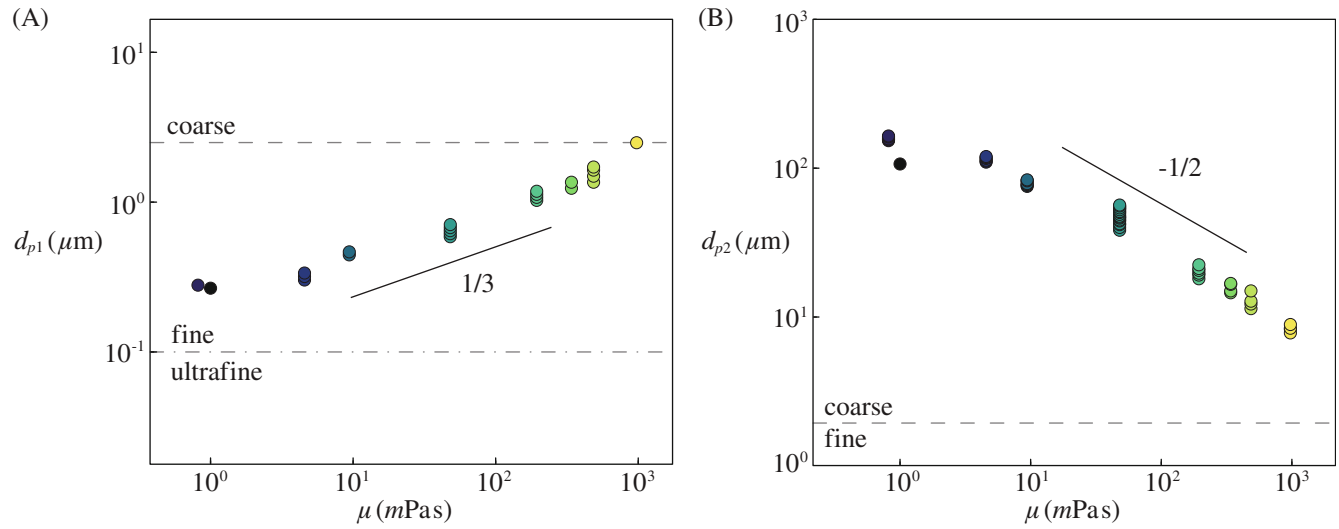

FIGURE 4 (A) Particle diameter associated with the (A) first minimum in scavenging efficiency d_{p1} and (B) second minimum in scavenging efficiency d_{p2} versus drop viscosity for $R = 0.1$ mm. The black marker shows an experiment from Grünig et al.[48] for water and $R = 0.5$ mm. The solid black lines are visual guides with slope 1/3 and $-1/2$.

shear from the surrounding air slows the drop, requiring smaller particles to match its velocity. These findings highlight viscosity as a tunable parameter for enhancing particle scavenging, particularly by extending the diffusion-dominated range. This added degree of control makes fiber-guided drops a versatile method for liquid distribution: by varying viscosity across fibers—for instance, alternating high- and low-viscosity solutions—different particle sizes can be selectively targeted within the same system.

Figure 5 shows the scavenging coefficient at the first minimum E_{p1} against the corresponding particle diameter d_{p1} for all experiments. Drop viscosity increases with marker shading, from dark blue to light yellow. As expected from the full scavenging curves (cf. Figure 3), higher viscosity increases drop residence time t_r, enhancing scavenging and shifting d_{p1} to larger values. Less obvious is the scatter in E_{p1} at fixed μ. The inset of Figure 5 plots E_{p1} versus drop spacing λ for $\mu = 48$ mPa s, showing a clear negative trend: smaller λ increases drop number density Γ, which improves scavenging. In practice, decreasing λ simply requires one to increase the flowrate Q, as shown in Supplemental Movie S1. These results demonstrate that drop residence time and drop number density—tuned via μ and λ, respectively—are the primary control parameters for optimizing fiber-guided drop scrubbers.

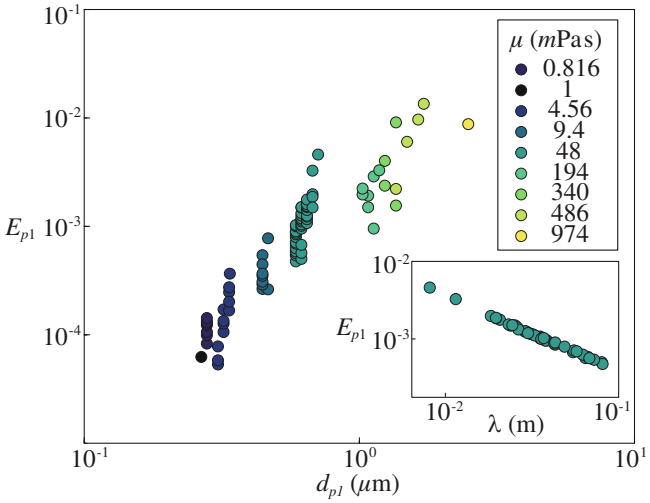

FIGURE 5 Particle scavenging coefficient at the first minimum E_{p1} against particle diameter d_{p1} for drop viscosities increasing as marker shading transitions from dark (blue) to light (yellow), and $R = 0.1$ mm. Inset shows E_{p1} against spacing between fiber drops λ for all data with $\mu = 48$ mPa s. The black marker shows data from Grünig et al.[48] for water and $R = 0.5$ mm.

5 | DISCUSSION

The central thesis of this work is that particle scavenging improves when falling drops are slowed using a fiber guide. We have identified the key factors influencing the scavenging coefficient and now seek to understand how these factors combine to determine E_{p1}. In Figure 5, E_{p1} did not collapse onto a single curve when plotted against d_{p1} alone, due to the influence of drop spacing. However, Figure 6A shows that plotting E_{p1} against the scaled particle diameter d_{p1}/λ collapses the data onto a single power-law trend with exponent 1.05 and $R^2 = 0.99$. This nondimensional relationship links scavenging efficiency to the associated particle size while accounting for the number of drops available for capture. Building on this result, we aim to express E_{p1} in terms of the two factors shown to most strongly enhance scavenging in our results: the drop residence time t_r and the drop number density Γ.

The particle size at the first minimum scales with viscosity $d_{p1} \sim \mu^{1/3}$, as shown earlier. Since drop velocity decreases with

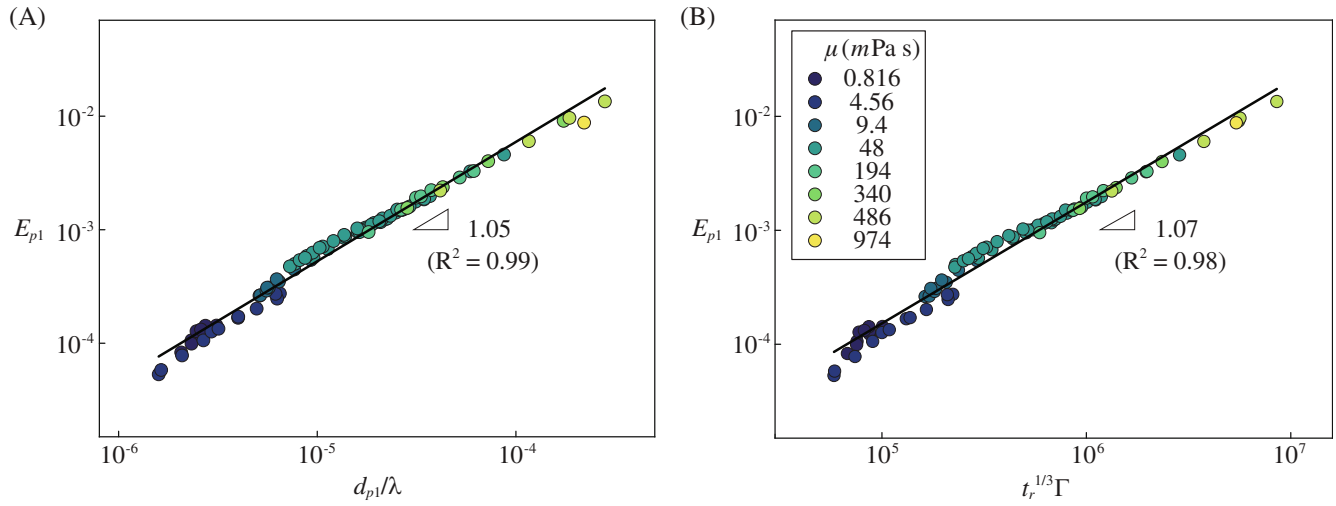

FIGURE 6 (A) Scavenging coefficient at the first minimum E_{p1} versus scaled particle diameter d_{p1}/λ, and (B) versus $t_r^{1/3}\,\Gamma$, for drops with $R = 0.1$ mm and increasing viscosity, indicated by marker shading, from dark blue to light yellow. Solid black lines are linear fits.

viscosity as $V_d \sim 1/\mu$, the residence time increases as $t_r = \mathcal{L}/V_d \sim \mu$ for a scrubber of fixed length $\mathcal{L}$. Combining these scalings gives $d_{p1} \sim t_r^{1/3}$. Additionally, the drop number density scales inversely with drop spacing $\Gamma \sim 1/\lambda$. Substituting these relations into $E_{p1} \sim d_{p1}/\lambda$ yields a new predictive form: $E_{p1} \sim t_r^{1/3}\,\Gamma$. Figure 6B confirms this prediction, showing that the data collapse onto a power-law trend with slope 1.07 and $R^2 = 0.98$. This result supports our central thesis: fiber-guided drops enhance wet scrubber performance by increasing residence time and provide precise control over the drop number density.

5.1 | Practical implications

This study provides actionable guidelines for designing more efficient wet scrubbers using fiber-guided drops. Our key finding is $E_{p1} \sim t_r^{1/3}\,\Gamma$, and suggests that scrubber efficiency can be improved by increasing drop residence time t_r and the drop number density Γ. These parameters can be readily tuned by adjusting drop viscosity, flowrate (drop spacing), and fiber spacing, enabling designers to target fine and ultrafine particles, those most detrimental to human health and commonly missed by conventional wet scrubbers operating in the Greenfield gap. Moreover, these improvements can be achieved within a more compact and energy-efficient design, as the ability to increase t_r reduces reliance on tall scrubber columns. While these results considered only the primary fiber-guided drops, experiments revealed the formation of smaller secondary drops (cf. Figure 1B). These secondary drops were excluded from simulations but likely enhance scavenging by increasing the effective drop number density and providing additional surface area for particle capture. Their presence may also help mitigate the second efficiency minimum, E_{p2}, by introducing a second drop size with a velocity that differs from the primary drops at E_{p2}.

In practice, increasing residence time by adjusting drop viscosity may not always be feasible or desirable. In such cases, the fiber radius R offers a practical alternative for controlling drop velocity, as larger radii correspond to slower-moving drops.[22] For finer control over the drop velocity V_d, the fiber's microstructure can be modified—for example, by using twisted or bundled fibers—which has been shown to influence drop motion[38,57,58] but may also suppress drop formation.[59] An additional complexity not explored here is that most wet scrubbers operate under airflow. This will likely alter scavenging efficiency, as strong counterflow can alter drop velocity.[26,49] A crossflow can cause drops to lose their symmetry, thereby also altering their dynamics,[36] and wakes produced around drops may restructure the global drop arrangement[60] and affect drop shape.[61–63] These combined fiber and airflow effects likely influence scavenging behavior and underscore the need for a pilot-scale system to evaluate performance under the complex, particle-laden flows typical of industrial exhaust. Our results offer both a design guide and an evaluation framework for such a system.

6 | CONCLUSION

We investigated the use of liquid drops flowing down vertical fibers as a novel strategy for liquid distribution in wet scrubbers. Through experiments with low-viscosity silicone oils, supplemented by high-viscosity data from prior work, we simulated particle collection efficiency across a wide range of drop viscosities μ and drop spacings λ. By comparing the performance of these fiber-guided drops to conventional free-falling drops, we demonstrated that fiber-guided configurations significantly enhance particle scavenging, especially within the Greenfield gap—an intermediate particle size range that is notoriously difficult to capture using traditional methods.

In particular, our results show that the minimum scavenging coefficient within this gap E_{p1} occurs at a particle size d_{p1} that increases with viscosity as $d_{p1} \sim \mu^{1/3}$. This shift moves the least-captured particle size toward larger diameters, thereby improving capture of the fine and ultrafine particles most hazardous to human health. A second minimum E_{p2} occurs when the particle and drop velocities match, and the associated particle size scales as $d_{p2} \sim \mu^{1/2}$. All values of E_{p1}

collapse onto a single curve when plotted against $t_r^{1/3}\Gamma$, highlighting the drop residence time and drop number density as the key variables that enhance scrubbing in fiber-guided systems. These findings demonstrate that fiber-guided drops offer a novel and effective pathway for improving the particle removal efficiency of wet scrubbers.

AUTHOR CONTRIBUTIONS

Chase T. Gabbard: formal analysis; data curation; methodology; investigation; visualization; writing – original draft; writing – review and editing. **James T. Rhoads:** data curation; methodology; visualization; writing – review and editing. **Joshua B. Bostwick:** conceptualization; project administration; supervision; resources; writing – review and editing; writing – original draft. **J. R. Saylor:** conceptualization; data curation; investigation; methodology; formal analysis; supervision; visualization; project administration; writing – original draft; writing – review and editing.

ACKNOWLEDGMENTS

C.T.G gratefully acknowledges the Hope Street Fellowship for support.

FUNDING INFORMATION

This work was supported in part by Clemson University through the Creative Inquiry Program.

CONFLICTS OF INTEREST

The authors report no conflict of interests.

DATA AVAILABILITY STATEMENT

The data presented in this work can be found in two files: Figs2 and3_Data.xls and Figs4thru6_Data.xls. The former has the E_p and E_p/E_{pw} data tabulated against d_p. A sheet within the file is provided for each of the viscosities explored here. The sheet name is the viscosity. The second file contains all of the data needed to reproduce Figures 4–6. Specifically, $d_{p1}, E_{p1}, d_{p2}, t_{res}, ND$, and λ are presented for each viscosity considered. These files can be downloaded from the following location: https://github.com/chase-gabbard/WetScrubber_FiberDrops.

ORCID

Chase T. Gabbard https://orcid.org/0009-0006-4412-4066
James T. Rhoads https://orcid.org/0009-0001-3084-7005
Joshua B. Bostwick https://orcid.org/0000-0001-7573-2108
J. R. Saylor https://orcid.org/0000-0001-9216-4712

REFERENCES

1. Anderson J, Thundiyil J, Stolbach A. Clearing the air: a review of the effects of particulate matter air pollution on human health. *J Med Toxicol*. 2012;8:166-175.
2. Greenfield S. Rain scavenging of radioactive particulate matter from the atmosphere. *J Atmos Sci*. 1957;14(2):115-125.
3. Davies R. Wettability and the capture, carriage and deposition of particles by raindrops. *Nature*. 1961;191(4788):616-617.
4. Green B, Dettmann M, Yli-Panula E, Rutherford S, Simpson R. Atmospheric Poaceae pollen frequencies and associations with meteorological parameters in Brisbane, Australia: a 5-year record, 1994–1999. *Int J Biometeorol*. 2004;48:172-178.
5. Idris N, Le-Minh N, Hayes J, Stuetz R. Performance of wet scrubbers to remove VOCs from rubber emissions. *J Environ Manag*. 2022;305:114426.
6. Danzomo B, Salami MJ, Jibrin S, Khan M, Nor I. Performance evaluation of wet scrubber system for industrial air pollution control. *ARPN J Eng Appl Sci*. 2012;7:1669-1677.
7. Bigu J, Grenier M, Hardcastle S. Effectiveness of a wet scrubber in reducing radioactive aerosol and dust concentrations in underground uranium mines. *Am Ind Hyg Assoc J*. 1988;49(11):572-578.
8. Onnen J. Wet scrubbers tackle pollution. *Environ Sci Technol*. 1972;6(12):994-998.
9. Sadeghpour A, Oroumiyeh F, Zhu Y, et al. Experimental study of a string-based counterflow wet electrostatic precipitator for collection of fine and ultrafine particles. *J Air Waste Manage Assoc*. 2021;71(7):851-865.
10. Schifftner KC, Hesketh HE. *Wet Scrubbers*. second ed. Technomic Publishing AG; 1996.
11. Zhao M, Xue P, Liu J, Liao J, Guo J. A review of removing SO2 and NOX by wet scrubbing. *Sustain Energy Technol Assess*. 2021;47:101451.
12. Parker KR. Why an electrostatic precipitator? *Springer*. 1997;1-10.
13. Meikap B, Biswas M. Fly-ash removal efficiency in a modified multistage bubble column scrubber. *Sep Purif Technol*. 2004;36(3):177-190.
14. Jones WP. Development of the venturi scrubber. *Ind Eng Chem*. 1949;41(11):2424-2427.
15. Fredericks S, Saylor JR. Parametric investigation of two aerosol scavenging models in the inertial regime. *J Aerosol Sci*. 2016;101:34-42.
16. Lemaitre P, Sow M, Quérel A, et al. Contribution of phoretic and electrostatic effects to the collection efficiency of submicron aerosol particles by raindrops. *Atmos*. 2020;11(10):1028.
17. Wang X, Zhang L, Moran MD. Uncertainty assessment of current size-resolved parameterizations for below-cloud particle scavenging by rain. *Atmos Chem Phys*. 2010;10:5685-5705.
18. Pruppacher H, Klett J. *Microphysics of Clouds and Precipitation*. Reidel Publishing Company; 1978.
19. Atlas D, Ulbrich CW. Path and area-integrated rainfall measurement by microwave attenuation in the 1-3 cm band. *J Appl Meteorol*. 1977;16:1322-1331.
20. Plateau J. *Statique expérimentale et théorique des liquides soumis aux seules forces moléculaires*. Gauthier-Villars; 1873.
21. Lord Rayleigh FRS On the instability of jets. *Proc Lond Math Soc*. 1878;1(1):4-13.
22. Gabbard C, Bostwick J. Scaling analysis of the Plateau–Rayleigh instability in thin film flow down a fiber. *Exp Fluids*. 2021;62(7):141.
23. Hattori K, Ishikawa M, Mori Y. Strings of liquid beads for gas-liquid contact operations. *AICHE J*. 1994;40(12):1983-1992.
24. Chinju H, Uchiyama K, Mori Y. String-of-beads flow of liquids on vertical wires for gas absorption. *AICHE J*. 2000;46(5):937-945.
25. Uchiyama K, Migita H, Ohmura R, Mori Y. Gas absorption into string-of-beads liquid flow with chemical reaction: application to carbon dioxide separation. *Int J Heat Mass Transf*. 2003;46(3):457-468.
26. Migita H, Soga K, Mori Y. Gas absorption in a wetted-wire column. *AICHE J*. 2005;51(8):2190-2198.
27. Wagstaff C, Al-Juaied M, Prabhudharwadkar D, Roberts W. Wetted-wire columns: a potential alternative to packed or spray columns. *Rev Chem Eng*. 2024;40(5):601-622.
28. Sadeghpour A, Zeng Z, Ji H, Dehdari Ebrahimi N, Bertozzi A, Ju Y. Water vapor capturing using an array of traveling liquid beads for desalination and water treatment. *Sci Adv*. 2019;5(4):eaav7662.
29. Zeng Z, Sadeghpour A, Ju Y. A highly effective multi-string humidifier with a low gas stream pressure drop for desalination. *Desalination*. 2019;449:92-100.

30. Kliakhandler I, Davis S, Bankoff S. Viscous beads on vertical fibre. *J Fluid Mech*. 2001;429:381-390.
31. Duprat C, Ruyer-Quil C, Kalliadasis S, Giorgiutti-Dauphiné F. Absolute and convective instabilities of a viscous film flowing down a vertical fiber. *Phys Rev Lett*. 2007;98(24):244502.
32. Duprat C, Ruyer-Quil C, Giorgiutti-Dauphiné F. Spatial evolution of a film flowing down a fiber. *Phys Fluids*. 2009;21(4):042109.
33. Gabbard C, Bostwick J. Asymmetric instability in thin-film flow down a fiber. *Phys Rev Fluids*. 2021;6(3):034005.
34. Eghbali S, Keiser L, Boujo E, Gallaire F. Whirling instability of an eccentric coated fibre. *J Fluid Mech*. 2022;952:A33.
35. Gabbard C, Bostwick J. Bead-on-fibre morphology in shear-thinning flow. *J Fluid Mech*. 2023;961:A14.
36. Cazaubiel A, Carlson A. Influence of wind on a viscous liquid film flowing down a thread. *Phys Rev Fluids*. 2023;8(5):054002.
37. Sadeghpour A, Zeng Z, Ju Y. Effects of nozzle geometry on the fluid dynamics of thin liquid films flowing down vertical strings in the Rayleigh–Plateau regime. *Langmuir*. 2017;33(25):6292-6299.
38. Leonard M, Van Hulle J, Weyer F, Terwagne D, Vandewalle N. Droplets sliding on single and multiple vertical fibers. *Physical Review Fluids*. 2023;8(10):103601.
39. Gabbard C, Rhoads J, Delhaye JM, Bostwick J. Scaling analysis for the frequency of Ostwaldian and Newtonian bead-on-fibre flows. *J Fluid Mech*. 2025;1002:A12.
40. Frenkel A. Nonlinear theory of strongly undulating thin films flowing down vertical cylinders. *Europhys Lett*. 1992;18(7):583-588.
41. Trifonov Y. Steady-state traveling waves on the surface of a viscous liquid film falling down on vertical wires and tubes. *AICHE J*. 1992;38(6):821-834.
42. Craster R, Matar O. On viscous beads flowing down a vertical fibre. *J Fluid Mech*. 2006;553:85-105.
43. Ruyer-Quil C, Treveleyan P, Giorgiutti-Dauphiné F, Duprat C, Kalliadasis S. Modelling film flows down a fibre. *J Fluid Mech*. 2008;603:431-462.
44. Novbari E, Oron A. Energy integral method model for the nonlinear dynamics of an axisymmetric thin liquid film falling on a vertical cylinder. *Phys Fluids*. 2009;21(6):062107.
45. Ji H, Sadeghpour A, Ju Y, Bertozzi A. Modelling film flows down a fibre influenced by nozzle geometry. *J Fluid Mech*. 2020;901:R6.
46. Zeng Z, Sadeghpour A, Warrier G, Ju Y. Experimental study of heat transfer between thin liquid films flowing down a vertical string in the Rayleigh-Plateau instability regime and a counterflowing gas stream. *Int J Heat Mass Transf*. 2017;108:830-840.
47. Zeng Z, Sadeghpour A, Ju Y. Thermohydraulic characteristics of a multi-string direct-contact heat exchanger. *Int J Heat Mass Transf*. 2018;126:536-544.
48. Grünig J, Lyagin E, Horn S, Skale T, Kraume M. Mass transfer characteristics of liquid films flowing down a vertical wire in a counter current gas flow. *Chem Eng Sci*. 2012;69(1):329-339.
49. Grünig J, Skale T, Kraume M. Liquid flow on a vertical wire in a countercurrent gas flow. *Chem Eng J*. 2010;164(1):121-131.
50. Ali M, Pasic H, Alam K, et al. Experimental study of cross-flow wet electrostatic precipitator. *J Air Waste Manage Assoc*. 2016;66(12):1237-1244.
51. Wagstaff C, Gubba SR, Truscott T, Algashgari K, Roberts WL. Wire density for a wetted-wire column. *Chem Eng Sci*. 2023;273:118633.
52. Gabbard C, Bostwick J. Gravity-driven flow of liquid bridges between vertical fibres. *J Fluid Mech*. 2024;997:A74.
53. Kyung SY, Jeong SH. Particulate-matter related respiratory diseases. *Tuberc Respir Dis*. 2020;83(2):116.
54. Harris SJ, Maricq MM. Signature size distributions for diesel and gasoline engine exhaust particulate matter. *J Aerosol Sci*. 2001;32(6):749-764.
55. Richards J. Control of particulate matter emissions. *APTI Course*. 2020;413.
56. Speirs N, Belden J, Hellum A. The capture of airborne particulates by rain. *J Fluid Mech*. 2023;958:A40.
57. Kern V, Carlson A. Twisted fibers enable drop flow control and enhance fog capture. *Proc Natl Acad Sci USA*. 2024;121(32):e2402252121.
58. Van Hulle J, Delforge C, Léonard M, Follet E, Vandewalle N. Droplet helical motion on twisted fibers. *Langmuir*. 2024;40(48):25413-25419.
59. Gabbard CT, Rhoads JT, Bostwick JB. Suppressing capillary instability in falling liquid threads. *J Fluid Mech*. 2024;1000:A77.
60. Wilson JL, Pahlavan AA, Erinin MA, Duprat C, Deike L, Stone HA. Aerodynamic interactions of drops on parallel fibres. *Nat Phys*. 2023;19(11):1667-1672.
61. Saylor JR, Jones BK. The existence of vortices in the wakes of simulated raindrops. *Phys Fluids*. 2005;17(4):31706–31706.
62. Jones BK, Saylor JR. Axis ratios of water drops levitated in a vertical wind tunnel. *J Atmos Ocean Technol*. 2009;26:2413-2419.
63. Fredericks S, Saylor JR. Experimental study of drop shape and wake effects on particle scavenging for non-evaporating drops using ultrasonic levitation. *J Aerosol Sci*. 2019;127:1-17.

SUPPORTING INFORMATION

Additional supporting information can be found online in the Supporting Information section at the end of this article.

How to cite this article: Gabbard CT, Rhoads JT, Bostwick JB, Saylor JR. Improving wet scrubber efficiency using fiber-guided drops. *AIChE J*. 2025;e70062. doi:10.1002/aic.70062